Acta Pharmaceutica Sinica B 2023;13(12):4893–4905

Chinese Pharmaceutical Association
Institute of Materia Medica, Chinese Academy of Medical Sciences

Acta Pharmaceutica Sinica B

www.elsevier.com/locate/apsb
www.sciencedirect.com

ORIGINAL ARTICLE

A unique binding pocket induced by a noncanonical SAH mimic to develop potent and selective PRMT inhibitors

Youchao Deng[a,#,†], Xiaosheng Song[b,†], Iredia D. Iyamu[a], Aiping Dong[b], Jinrong Min[b,c,*], Rong Huang[a,*]

[a]*Department of Medicinal Chemistry and Molecular Pharmacology, Center for Cancer Research, Institute for Drug Discovery, Purdue University, West Lafayette, IN 47907, USA*
[b]*Structural Genomics Consortium and Department of Physiology, University of Toronto, Toronto, Ontario M5G 1L7, Canada*
[c]*Hubei Key Laboratory of Genetic Regulation and Integrative Biology, School of Life Sciences, Central China Normal University, Wuhan 430079, China*

Received 27 April 2023; received in revised form 9 July 2023; accepted 17 July 2023

KEY WORDS

PRMTs;
Structure based inhibitor design;
Benzyl urea;
Noncanonical SAH mimic;
Homocysteine binding pocket;
Crystal structure

Abstract Protein arginine methyltransferases (PRMTs) are attractive targets for developing therapeutic agents, but selective PRMT inhibitors targeting the cofactor SAM binding site are limited. Herein, we report the discovery of a noncanonical but less polar SAH surrogate YD1113 by replacing the benzyl guanidine of a pan-PRMT inhibitor with a benzyl urea, potently and selectively inhibiting PRMT3/4/5. Importantly, crystal structures reveal that the benzyl urea moiety of YD1113 induces a unique and novel hydrophobic binding pocket in PRMT3/4, providing a structural basis for the selectivity. In addition, YD1113 can be modified by introducing a substrate mimic to form a "T-shaped" bisubstrate analogue YD1290 to engage both the SAM and substrate binding pockets, exhibiting potent and selective inhibition to type I PRMTs ($IC_{50} < 5$ nmol/L). In summary, we demonstrated the promise of YD1113 as a general SAH mimic to build potent and selective PRMT inhibitors.

*Corresponding authors.
E-mail addresses: minjinrong@ccnu.edu.cn (Jinrong Min), huang-r@purdue.edu (Rong Huang).
[†]These authors made equal contributions to this work.
[#]Current address: Xiangya School of Pharmaceutical Sciences, Central South University, Changsha 410013, China.
Peer review under the responsibility of Chinese Pharmaceutical Association and Institute of Materia Medica, Chinese Academy of Medical Sciences.

https://doi.org/10.1016/j.apsb.2023.07.022

1. Introduction

Protein arginine methyltransferases (PRMTs) transfer the methyl group from the cofactor *S*-adenosyl-L-methionine (SAM) to the guanidine group on arginine residues while generating *S*-adenosyl-L-homocysteine (SAH) and methylated proteins. There are three types of PRMTs according to their methylation products. Type I (PRMT 1, 2, 3, 4, 6, and 8) catalyze mono- and asymmetric di-methylation on arginine. Type II (PRMT 5 and 9) produce mono- and symmetric di-methylation on arginine. Type III (PRMT 7) only monomethylates arginine[1]. Abnormal expression or activity of PRMTs has been involved in various diseases, including cancers, cardiovascular diseases, inflammatory diseases, and diabetes[2−6]. SAH has been pursued as a lead compound to build potent inhibitors for methyltransferases. Not surprisingly, selectivity is a central challenge for SAH mimics. Nevertheless, several PRMT inhibitors of SAH or sinefungin analogues have been successfully developed (Fig. 1). For instance, a PRMT5 inhibitor JNJ-64619178 is currently in clinical trials for patients with advanced solid tumors, non-Hodgkin's lymphoma, and lower-risk myelodysplastic syndrome[7]. SGC8158 is a selective PRMT7 inhibitor[8]. Recently, we developed a PRMT pan-inhibitor II757 by connecting the adenosine and guanidine moieties[9].

However, most SAH-based PRMT inhibitors comprise 5′-thioadenosine or its mimic and a guanidine function group, losing interactions with the homocysteine binding channel. One reason is the polarity of the α-amino acid moiety causing low cellular uptake. Another reason is the challenge of identifying less polar surrogates to fit into a deep narrow binding channel while retaining the key interactions. Notably, the α-amino acid moiety of the homocysteine forms multiple interactions with the methyltransferases and contributes significantly to the cofactor SAM binding. Therefore, the discovery of a homocysteine mimic would be beneficial to boost the potency of SAH-based inhibitors for methyltransferases. To date, two cases have been reported. One example is the PRMT4 inhibitor SKI-72, a sinefungin derivative with a benzylamine to occupy the α-amino carboxylate moiety of the SAH binding site according to the co-crystal structure (PDB ID: 6D2L)[10]. Another example is the PRMT4 bisubstrate inhibitor that bears a 2-aminopyrimidine or 2-aminopyridine, alternatively occupying either the α-amino carboxylate moiety of SAH or the substrate arginine binding site (PDB ID: 6S74, 6S7A)[11].

2. Results and discussion

Recently, we reported a series of PRMT inhibitors that connect 5′-thioadenosine with a tripeptide through a substituted guanidine group[6,12]. To dissect the binding mode, we obtained the co-crystal structures of PRMT3 complexed with II710 (**1a**, IC_{50} = 12 μmol/L for PRMT3) (Fig. 2). The overall topology of the PRMT3−II710 complex aligned well with the reported co-crystal structure of the PRMT3−SAH (PDB ID: 2FYT), which clearly showed II710 as a bisubstrate analogue residing in the active site of PRMT3 (Fig. 2a). Specifically, the thioadenosine moiety of II710 aligned well with the adenosine moiety of SAH, forming hydrogen bonds with Asp285, Gln286, Ile313, and Glu314. The benzyl guanidine group protrudes into the arginine binding channel to interact with Glu329, Tyr333, and His479 (Fig. 2b), confirming the bisubstrate feature of inhibition. Compared to SAH, II710 had no interaction with the homocysteine binding site (Fig. 2c−d).

To enhance the inhibition, we designed and synthesized II710 analogues by exploring the linker and substitution on the guanidine group (Scheme 1). Specifically, we replaced the guanidino group with a urea group to afford **1b**, inspired by the PRMT 5/7 dual inhibitor DS437 bearing a 2-C atom linker between the 5′-thioadenosine and urea group[13]. However, **1b** only inhibited 50% of PRMT3 activity at 70 μmol/L. Given the importance of the linker length for the bisubstrate analogues[14,15]. we reduced the linker from a 3C- to 2C-atom to produce YD1113 (**1c**), resulting in 140-fold increased inhibition for PRMT3. However, a similar modification in II710 generated **1d** containing a 2C-atom linker, causing a 3-fold decrease. Next, we examined the effect of substitutions on the urea moiety of YD1113 (Table 1). Briefly, introducing a 4-fluoro (**1e**) group to the benzyl group of YD1113 led to an over 10-fold reduction. Replacement of the benzyl group

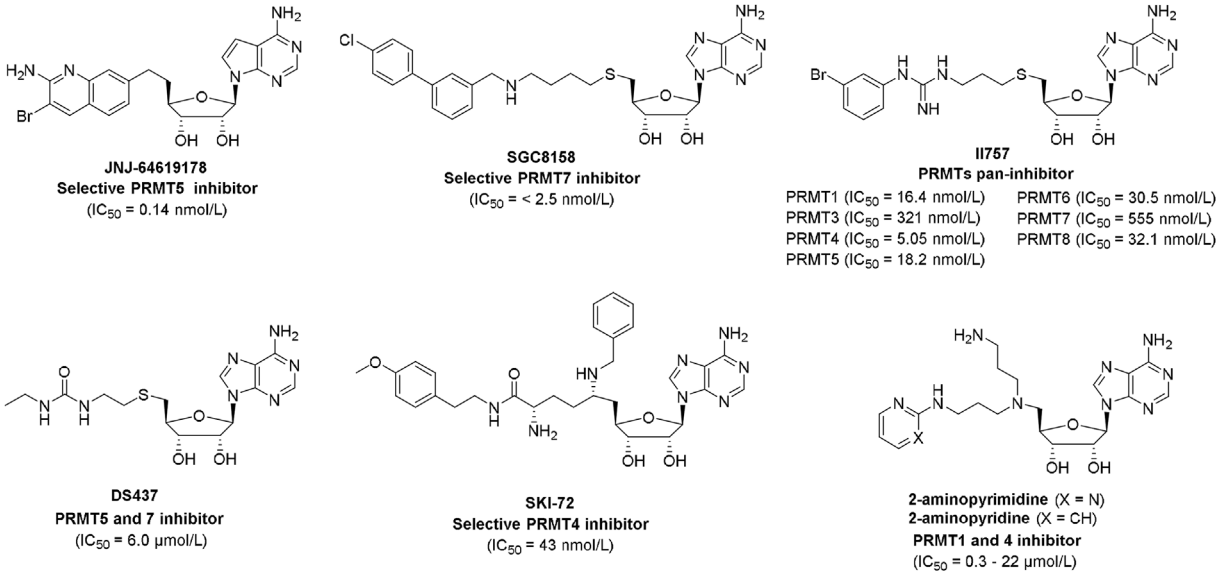

Figure 1 Structures of the representative PRMTs inhibitors.

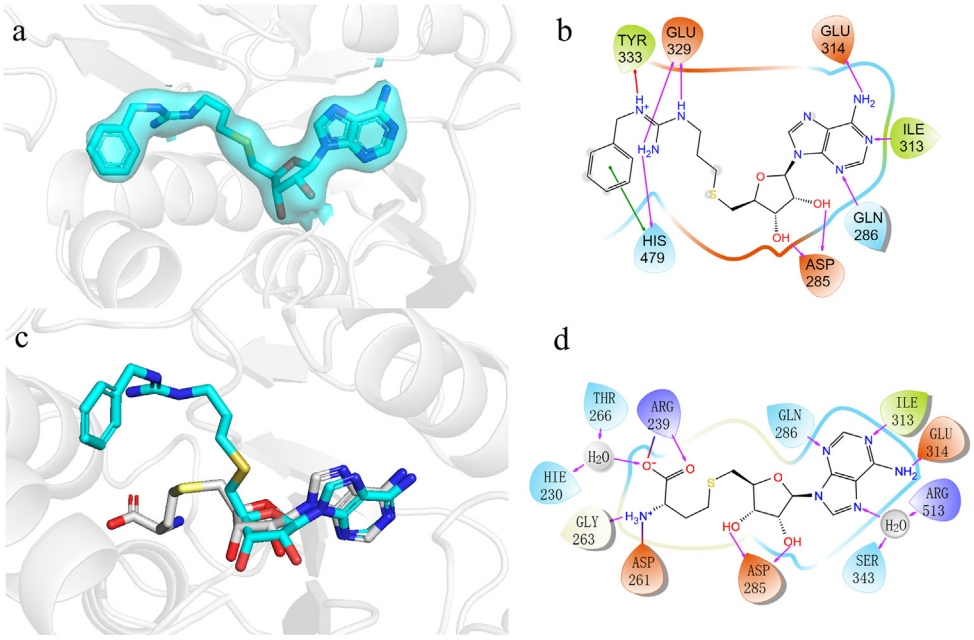

Figure 2 The complex structure of PRMT3 (gray cartoon) with II710 (light blue stick, PDB ID: 8G2F) or SAH (gray stick, PDB ID: 2FYT). (a, b) Detailed interactions of II710 with PRMT3 in the complex structures. A $2Fo-Fc$ omit map contoured at 1.0 σ is shown for II710 as a transparent turquoise isosurface. (c) Structure alignment of II710 and SAH. (d) 2D interaction diagram of SAH with PRMT3. The annotation is based on UniProt. ILE313 is corresponded to ILE330 in PDB 2FYT.

with phenylethyl (**1f**) or phenylpropyl (**1g**) abolished the inhibition activity (>100 μmol/L). Whereas replacing the benzyl ring of YD1113 with phenyl (**1h**) or *para*-fluorophenyl ring (**1i**) only led to a 4-fold decreased inhibition, a *para*-chlorophenyl (**1j**) reduced 10-fold compared to **1i** with a fluoride substitution. Not surprisingly, naphthalene (**1k**) caused over 40-fold reduction compared to phenyl (**1h**). The decreased activity of **1c** to **1g** and **1h** to **1k** indicated that the binding site of the benzyl urea group is sensitive to the steric effects, implying a narrow space. However, **1l** and **1m** with ethyl and cyclohexane groups showed IC_{50} values

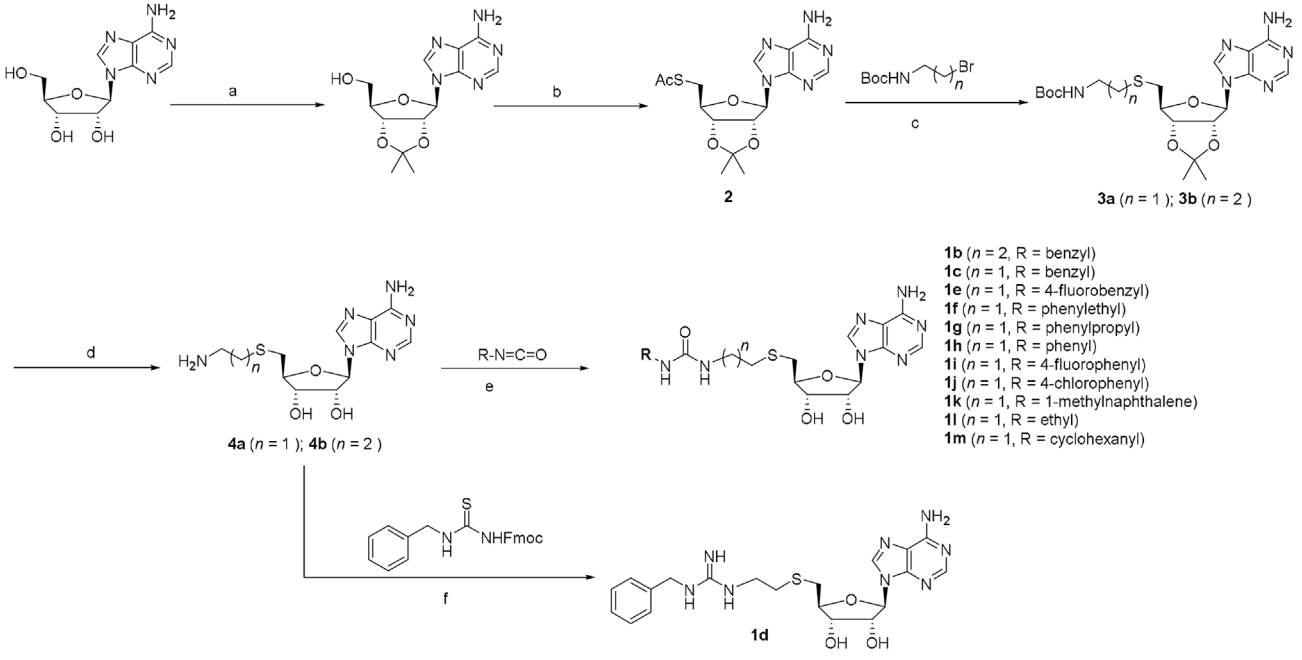

Scheme 1 Synthesis of urea analogues. Reagents and conditions: (a) pTsOH, triethyl orthoformate, acetone, rt, overnight, 89%; (b) thioacetic acid, PPh_3, DIAD, THF, 0 °C−rt, overnight, 91%; (c) NaOMe, MeOH, rt, overnight, 83%−84%; (d) TFA, H_2O, 0 °C−rt, 24 h, quantitative yield; (e) isocyanate, DMF, Et_3N, rt, 53%−88%; (f) EDC, DIPEA, DMF, 51%.

over 100 μmol/L, suggesting the benzyl ring of YD1113 may contribute to the binding by forming pi−pi or cation−pi interactions.

The sensitivity of YD1113 to the steric effects in the above SAR studies (Table 1) is inexplicable by a relatively open and tolerable peptide substrate binding channel of PRMTs[16]. This contradiction prompted us to hypothesize that YD1113 binds to an alternative pocket rather than acts as a bisubstrate analogue to reach the peptide binding pocket. We tested our hypothesis by investigating its inhibition mechanism with a SAHH-coupled fluorescence-based assay[17]. The IC_{50} values of YD1113 remained constant with the increased ratio of peptide/K_m (Fig. 3a−b) while increasing linearly with the ratio of SAM/K_m (Fig. 3c−d). This result demonstrated that YD1113 is competitive to SAM and noncompetitive to the peptide substrate of PRMT3, supporting our hypothesis. Thus, the urea substitution altered the binding mode of YD1113 compared to the guanidine analogue II710 with the bisubstrate feature, as YD1113 lost engagement with the peptide binding site.

Next, we investigated the selectivity of YD1113 on a panel of PRMTs at 10 μmol/L. YD1113 showed significant inhibition to PRMT3, 4, and 5 (>95%), moderate inhibition to PRMT7 (>75%), and limited inhibition to PRMT1, 6, and 8 (<35%) (Fig. 3e). As YD1113 exhibited over 50% inhibition for PRMT3, 4, 5, and 7 at 10 μmol/L, we then chose to determine the IC_{50} values of YD1113 for these four PRMTs. Indeed, YD1113 demonstrated a potent and comparable activity for PRMT3 and 5 with an IC_{50} value at 321 and 351 nmol/L, respectively. Moreover, YD1113 is 2-fold more potent for PRMT4 and 7-fold less potent for PRMT7 than PRMT3, respectively. In addition, we also checked its inhibition to our in-house methyltransferase panel along with SAH hydrolase. Indeed, YD1113 did not exhibit any inhibition for SAHH, lysine methyltransferases G9a and SETD7, nicotinamide *N*-methyltransferase (NNMT), and protein N-terminal methyltransferase 1 (NTMT1) (Supporting Information Fig. S1). Notably, both NNMT and NTMT1 also belong to Rossmann fold methyltransferases.

To understand the binding modes of YD1113, we determined the X-ray structures of PRMT3 and PRMT4 complexed with YD1113, respectively. The overall topology of the PRMT3-YD1113 complex is similar to those in the complex with SAH (Fig. 4). As illustrated in the electron density map, YD1113 only occupied the SAH binding site without interactions with the double E loop region located at the edge of the substrate peptide binding channel (Fig. 4a). Similar to SAH, the adenosine moiety of YD1113 interacted with Phe221, Asp285, Ile313, and Glu314 (Fig. 4b). The urea group bound at the same position as the α-amino carboxylate of SAH, forming similar interactions with Arg239, Gly263, and water (Fig. 4b−c). Strikingly, the benzyl urea reached into a hitherto unrecognized pocket adjacent to the binding pocket of α-amino carboxylate moiety of SAH (Fig. 4). Remarkably, the conformations of Arg239, Thr240, Ile268, and Leu269 were altered to create a hydrophobic pocket (Fig. 4d), where Arg239, Ile268, and Leu269 located at the entrance and stacked with the benzyl group in a sandwich manner. Meanwhile, Tyr243 at the bottom of the hydrophobic pocket formed a pi−pi interaction with the benzyl group. Furthermore, limited space in this new pocket provided a structural basis to explain why different substitutions on the benzyl ring of YD1113 substantially impacted its inhibitory activity on PRMT3 (Table 1). For example, the SARs studies supported that the pi−pi interaction between Tyr243 and the benzyl group was critical for binding, as exemplified by a dramatic decrease in binding with a cyclohexane or ethyl replacement. In summary, the co-crystal structure provided

Table 1 IC_{50} values of the synthesized urea compounds on PRMT3.

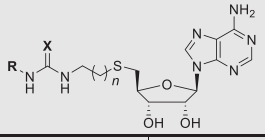

Compound ID	R	X	*n*	IC_{50} (μmol/L)	Compound ID	R	X	*n*	IC_{50} (μmol/L)
1a (II710)		NH	2	12 ± 1.3	1h		O	1	1.9 ± 0.12
1b		O	2	70 ± 11	1i		O	1	2.0 ± 0.23
1c (YD1113)		O	1	0.52 ± 0.07	1j		O	1	22 ± 2.9
1d		NH	1	33 ± 4.3	1k		O	1	81 ± 17
1e	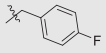	O	1	5.9 ± 1.4	1l		O	1	>100
1f		O	1	>100	1m		O	1	>100
1g	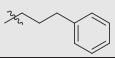	O	1	>100					

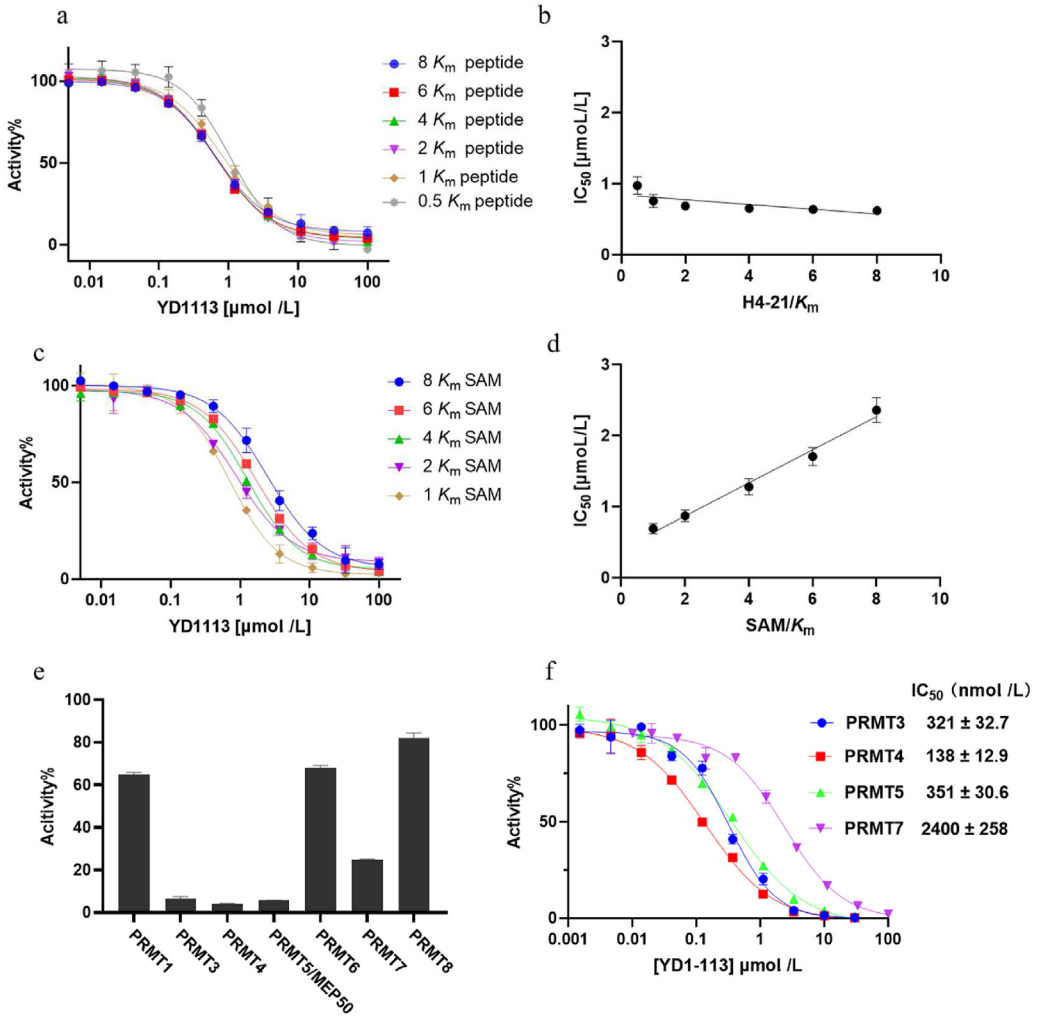

Figure 3 Inhibition mechanism and selectivity of YD1113. (a) IC_{50} curves of YD1113 at varying concentrations of peptide substrate H4-21 with a fixed concentration of SAM; (b) Linear regression plot of IC_{50} values for YD1113 with an increased ratio of peptide/K_m; (c) IC_{50} curves of YD1113 at varying concentrations of SAM with a fixed concentration of H4-21; (d) Plot of IC_{50} values for YD1113 with an increased ratio of SAM/K_m value. All the experiments were performed in triplicate ($n = 3$) and presented as mean ± SD. (e) Inhibition study of YD1113 on PRMT family members at 10 μmol/L at Reaction Biology Corp. Both SAM and substrates are at their physiological values. (f) IC_{50} determination of YD1113 on PRMT3, 4, 5 and 7 with both SAM and substrates at their respective physiological values by Reaction Biology Corp. All experiments were performed in duplicate ($n = 2$).

the first evidence that the benzyl urea functioned as a unique mimic for the α-amino carboxylate moiety of SAH for binding to PRMT3. This newly uncovered pocket does not exist in the previous structures of PRMT3 in complexes with SAH or II710. Thus, we attributed this uniquely induced binding pocket to the benzyl urea of YD1113.

Likewise, YD1113 displayed a similar binding pose in the active site of PRMT4. Briefly, the adenosine moiety of YD1113 forms hydrogen bonds with Gln159, Glu214, Ala215, Val242, and Glu243, and pi−pi interactions with Phe150 (Fig. 5a–c). Meanwhile, the urea group of YD1113 reaches the location where the carboxylic acid moiety of SAH resides, forming hydrogen bonds with Arg168 and water. In addition, the benzyl group of YD1113 protruded into a new hydrophobic pocket (formed by Arg168, Ile197, and Leu198) and created a pi−pi interaction with Tyr172 (Fig. 5b–d). This result further certifies that YD1113 acted as a unique surrogate of SAH by interacting with both the SAM binding pocket and a newly formed hydrophobic pocket.

As the key residues of the SAM binding pocket are conserved across all PRMT members[16], we speculated that a similar hydrophobic pocket may exist in all PRMTs. To investigate this prospect, we aligned the SAH binding pockets of all seven PRMTs with reported co-crystal structures in complex with SAH. Then we extracted the residues around the hydrophobic pocket as PRMT3 for comparison. Indeed, all type I PRMTs share identical residues (one Arg, two Ile, and one Tyr) at the same position (Supporting Information Table S1). Interestingly, PRMT7 has similar residues (Arg44, Leu77, Leu78, and Tyr48) at the same position as type I PRMTs. Compared to type I and III PRMTs, PRMT5 has similar residues despite minor differences. For instance, PRMT5 has a Tyr337 for the pi−pi interaction and a matching set of three residues with similar characteristics (Lys333, Pro370, and Leu371) to create a hydrophobic pocket. Although no X-ray structures have been obtained for YD1113 in complex with PRMT5/7, potent inhibition of YD1113 for PRMT5/7 ($IC_{50} < 2.4$ μmol/L) inferred that the benzyl group may induce and interact with a hydrophobic

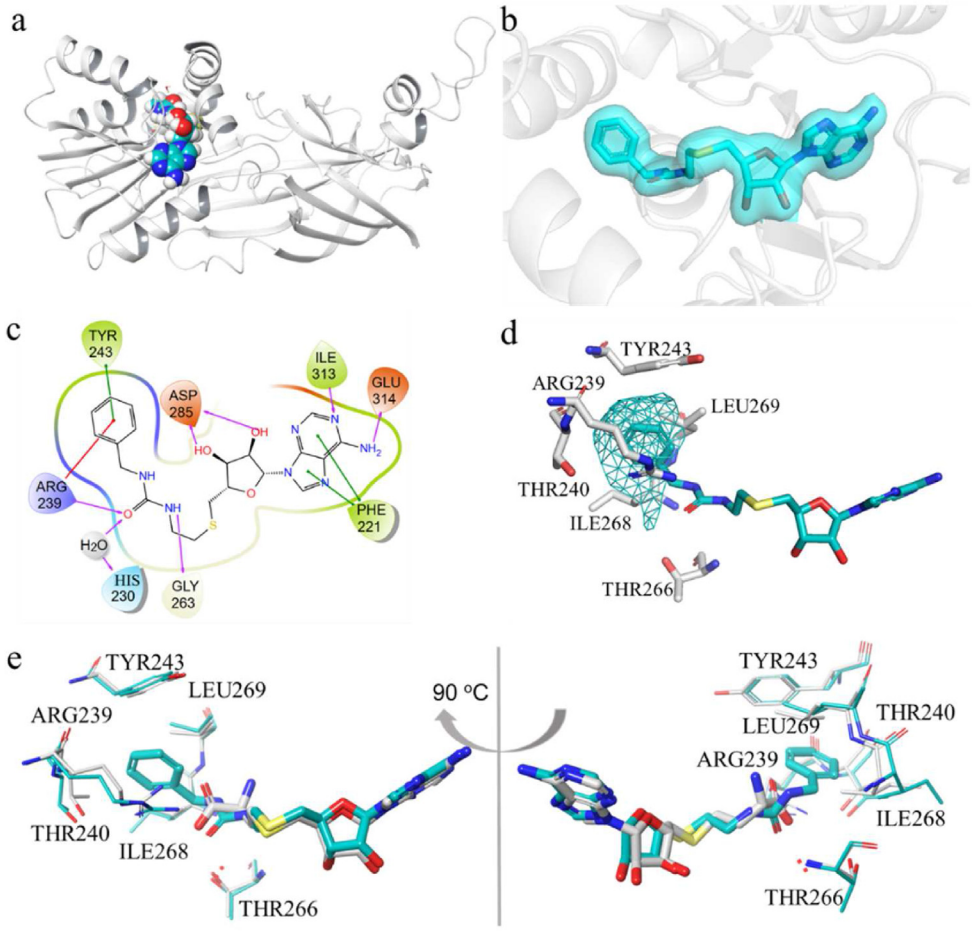

Figure 4 X-ray co-crystal structure of PRMT3 (gray cartoon) bound with YD1113 (light blue stick, PDB ID:8G2G) or SAH (gray stick, PDB ID: 2FYT). (a) overview of the X-ray structure of PRMT3 with YD1113. (b) A 2*F*o−*F*c omit map contoured at 1.0 σ is shown for YD1113as a transparent light blue isosurface. (c) Ligand interaction diagram of YD1113 with PRMT3. (d) The binding pocket of benzyl urea moiety of YD1113 (shown in the light blue mesh) in PRMT3. (e) Structure alignment of the key residues of the hydrophobic pocket. The residues of the SAH/YD1113-PRMT3 complex are gray and light blue sticks, respectively.

pocket as we observed in PRMT3/4. Altogether, it is reasonable to predict that a similar hydrophobic pocket adjacent to homocysteine commonly existed in all PRMTs, which the benzyl urea of YD1113 or similar analogues may induce. Even though the hydrophobic pocket exists in all PRMTs, it does not mean these pockets are identical, as YD1113 exhibited different inhibitory activity for each PRMT. In other words, the benzyl urea group may be fine-tuned further to increase the selectivity.

After validating the benzyl urea moiety as an unconventional homocysteine mimic of SAH for PRMTs, we hypothesize that incorporating the benzyl urea moiety into our previously reported pan PRMT inhibitor II757 would build a potent bisubstrate inhibitor[9]. Hence, YD1290 was designed to merge YD1113 and II757 to form a "T-shaped" (Fig. 6a). To enable a stable trisubstitution, we replaced the sulfur atom with a nitrogen atom. YD1290 was synthesized following the reported methods (Scheme 2)[9,15] and tested in a radioactivity assay for PRMTs (Fig. 6b). Like its parent compound II757, YD1290 demonstrated potency to all tested PRMTs. Compared to YD1113, YD1290 completely abolished PRMT4 activity even at 1.5 nmol/L and displayed >80-fold potency to PRMT1, 3, 4, 6, and 8. To date, YD1290 is the most potent inhibitor for type I PRMTs. It is noteworthy that the IC_{50} values of YD1290 for PRMT1−4, 6, and 8 are below half of enzyme concentration in the radioactive assay under the current conditions, indicating YD1290 is a tight inhibitor.

Next, we conducted the thermal shift assay (TSA) as an orthogonal method to examine the effects of YD1290 on the thermal stability of PRMT1, 3, and 4 (Supporting Information Fig. S2). Incubation of YD1290 with all three PRMTs induced a higher thermal stabilization (ΔT_m = +8.7, +23.4, and +10.9 °C) than the additive contributions of SAM (ΔT_m = +1.6, +1.1, +1.9 °C) and YD1113 (ΔT_m = +0.6, +5.8, +2.6 °C). These results suggested that YD1290 can significantly increase the thermal stability of the tested PRMTs, validating its interaction with PRMT1/3/4.

To confirm the potent inhibition activities of YD1290 on type I PRMTs resulting from bisubstrate characteristics, we determined its inhibition mechanism on PRMT1 through the SAHH-coupled fluorescence-based assay. Like II757 and YD1113, the IC_{50} values of YD1290 increased linearly with the ratio of SAM/K_m (Fig. 7a−b), indicating YD1290 is a SAM-competitive inhibitor. However, the IC_{50} of YD1290 was slightly increased when the ratio of peptide/K_m increased (Fig. 7c−d). These results demonstrated that YD1290 not only retained the SAM competitive ability as its

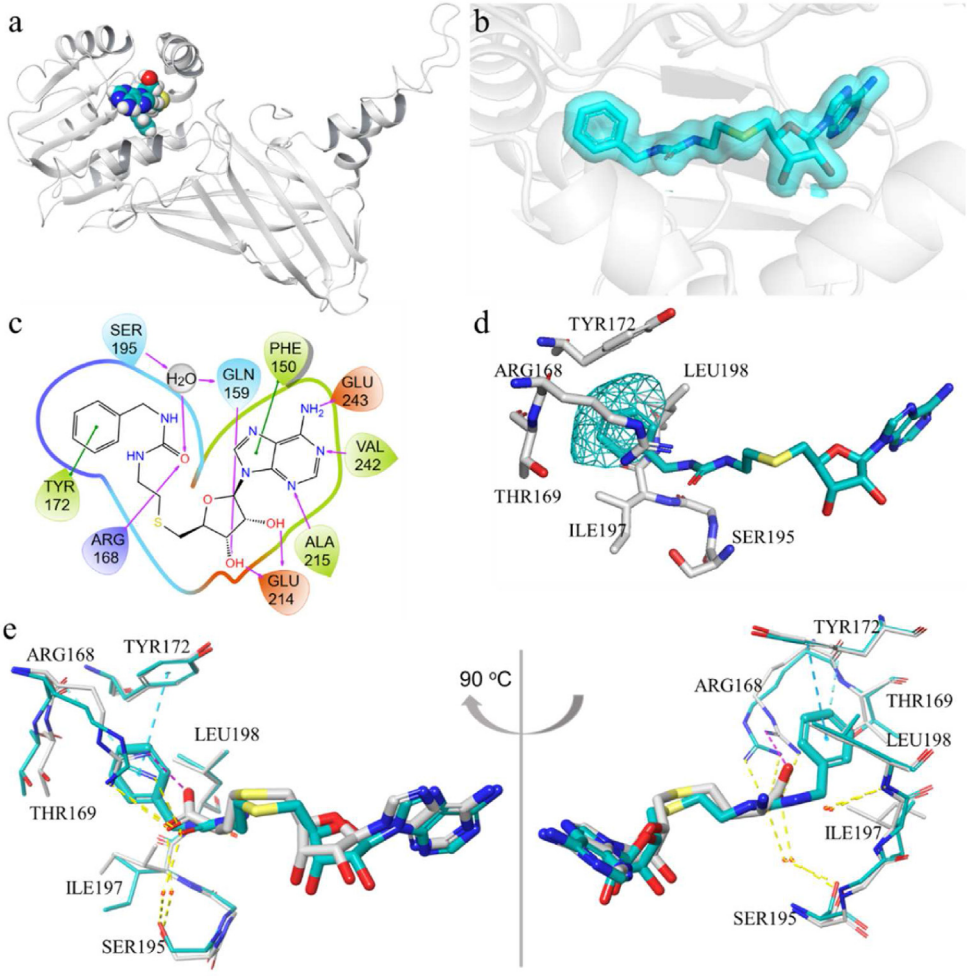

Figure 5 X-ray co-crystal structure of PRMT4 (gray cartoon) complexed with YD1113 (light blue stick, PDB ID:8G2H) or SAH (gray stick, PDB ID: 5IH3). (a) overview of the X-ray structure of PRMT4 bound with YD1113. (b) A 2*Fo*−*Fc* omit map contoured at 1.0 σ is shown for YD1113 as a transparent light blue isosurface. (c) Ligand interaction diagram of YD1113 with PRMT4. (d) The binding pocket of the benzyl urea moiety of YD1113 in PRMT4. And the binding pocket of the benzyl group was shown in the light blue mesh. (e) Structure alignment of the residues of the hydrophobic pocket. The residues of the SAH/YD1113−PRMT4 complex are gray and light blue sticks, respectively.

parent compounds YD1113 and II757, but also gained some interactions with the substrate peptide binding pocket as II757, as we hypothesized.

To further validate the binding mode of YD1290, we determined the co-crystal structure of PRMT4 complexed with YD1290. Indeed, YD1290 demonstrated a "T-shaped" binding mode in the active site by engaging with both SAM and peptide binding pockets (Fig. 8a). Like YD1113, the benzyl urea moiety of YD1290 imitated the homocysteine to interact with Gln159, Arg168, Tyr172, and Gly192 (Fig. 8b−c). Furthermore, the *meta*-bromobenzene guanidine of YD1290 located at the double E loop region interacted with Glu257 and Glu266, supporting the peptide substrate competitive ability of YD1290. In addition, the tertiary amine of YD1290 also formed a cation−pi interaction with Tyr153.

To examine the selectivity, we tested the inhibition of YD1290 on four in-house methyltransferases, including protein N-terminal methyltransferase 1 (NTMT1), nicotinamide *N*-methyltransferase (NNMT), and two protein lysine methyltransferases PKMT (G9a and SETD7). In addition, SAHH was included as it is used in the coupled fluorescence assay and possesses a SAH binding site. As shown in Fig. 8d, YD1290 did not display any significant inhibition to SAHH, NTMT1, SETD7, G9a, and NNMT at 100 μmol/L.

To evaluate the cell permeability ofYD1290, we examined its uptake by MDA-MB-231 cells using MALDI-MS after a 4-h incubation period. The compound was not observed in the cell lysates at concentrations of 100 and 10 μmol/L, but the control (cell permeable peptide) was taken up by the cells after 1 μmol/L for 1 h (Supporting Information Fig. S3). This result indicates poor permeability of YD1290, which needs to be optimized for cell-based studies.

3. Conclusions

In summary, we discovered and thoroughly verified that the benzyl urea moiety can function as an unconventional analogue of α-amino carboxylate moiety of SAH to retain the interaction with PRMTs. Our preliminary SAR data also indicates that the inhibition is sensitive to the substitution in the urea group. Among them, 2-(3-benzylureido)ethyl)thioadenosine (YD1113) is a non-canonical SAH mimic to interact with PRMTs. Our co-crystal structures of YD1113 complexed with PRMT3 or PRMT4 illustrated the molecular interaction, providing the first evidence to

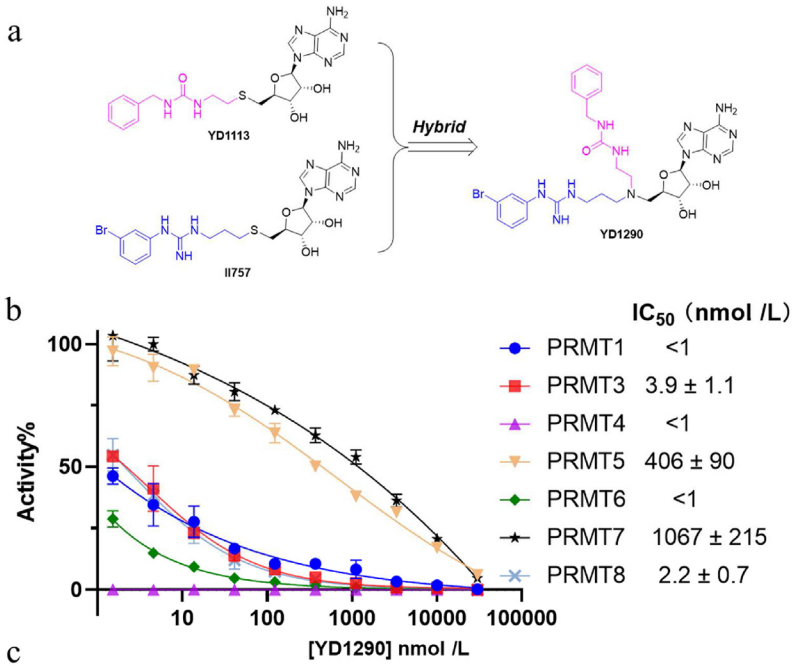

	PRMT1	PRMT3	PRMT4	PRMT5	PRMT6	PRMT7	PRMT8
II757	16	321	5	18	30	555	32
YD1113	> 10000	321	138	351	> 10000	2400	> 10000
YD1290	<1	4	<1	406	<1	1067	2

Figure 6 (a) A hybrid of YD1113 and II757 affords a "T-shaped" PRMT inhibitor YD1290. (b) Inhibition activity of YD1290 for a panel of PRMTs. (c) Comparison of IC_{50} values (nmol/L) of YD1290 with YD1113 and II757 under the same assay condition by Reaction Biology Corp. All experiments were performed in duplicate ($n = 2$).

confirm the biocompatibility of 3-ethyl-1-benzyl urea to mimic homocysteine. To date, few PRMT inhibitors engage the homocysteine binding channel. Notably, a PRMT 5/7 dual inhibitor DS437 was predicted to anchor in the homocysteine binding site but with no experimental evidence[13]. Our data boost the credibility of the projection of the urea group of DS437 to engage the homocysteine binding site[13].

Furthermore, we demonstrate that the benzyl urea moiety can be applied in developing "T-shaped" PRMT bisubstrate inhibitors to engage both SAM and peptide binding pockets. YD1290 is a

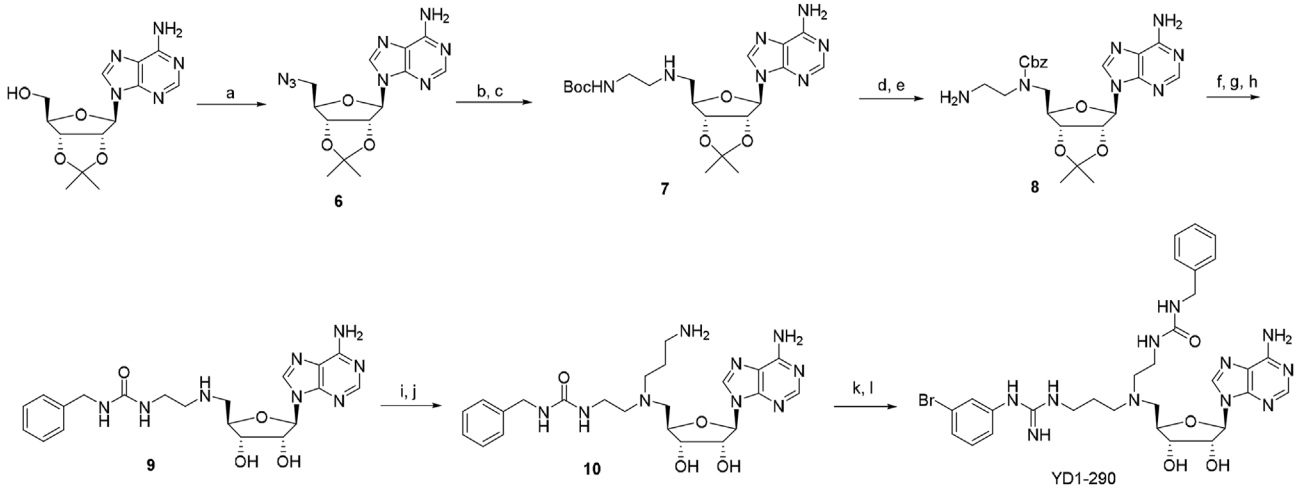

Scheme 2 Synthesis of YD1290. Reagents and conditions: (a) DPPA, DBU, anhydrous dioxane, NaN_3, 15-crown-5, reflux, 90%; (b) H_2, Pd/C, MeOH, rt, overnight; (c) *N*-Boc-2-aminoacetaldehyde, $NaBH_3CN$, MeOH, rt, 4 h, 82% in 2-stpes; (d) Cbz-Cl, K_2CO_3, THF, H_2O, 0 °C−rt, overnight; (e) TFA, DCM, rt, 1 h, 75% in two steps; (f) benzyl isocyanate, DCM, Et_3N, rt; (g) HCO_2H, 10% Pd/C, MeOH, reflux, 2 h; (h) TFA, H_2O, 0 °C−rt, 24 h, 61% in two steps; (i) *tert*-butyl *N*-(3-oxopropyl)carbamate, $NaBH_3CN$, MeOH, rt, 4 h; (j) TFA, DCM, rt, 4 h, 81% yield in two steps; (k) 1-(3-bromophenyl)-3-*N*-Fmoc-thiourea, EDC, DIPEA, DCM/DMF, rt, overnight; (l) piperidine, DCM, rt, 2 h, 43% yield in two steps.

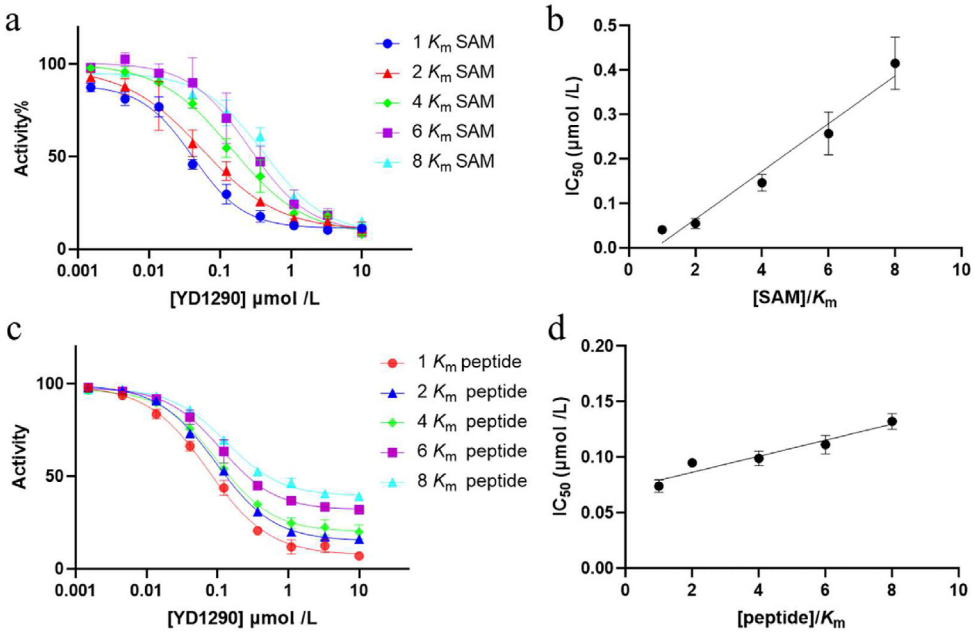

Figure 7 Inhibition mechanism of YD1290. (a, b) YD1290 is a SAM-site competitive inhibitor of PRMT1 as the IC_{50} value increases linearly with the ratio of SAM/K_m increasing. (c, d) YD1290 is a peptide-site competitive inhibitor of PRMT1 as the IC_{50} value slightly increases with the ratio of peptide/K_m increases. All experiments were performed in duplicate ($n = 3$).

potent and selective type I PRMT inhibitor, implying that the active site of type II PRMTs differs from those of type I PRMTs. Since YD1290 has limited cellular permeability, future investigation will focus on structural optimization to enhance cell uptake and cellular potency. Compared to SAH, YD1113 is less polar with the benzyl urea to replace the α-amino carboxylate moiety. Thus, YD1113 has the potential to serve as a building block to develop potent and selective inhibitors for PRMTs.

Interestingly, a similar hydrophobic pocket was created in DOT1L by the *tert*-butyl phenyl urea moiety of EPZ004777[18,19]. It is believed that the high selectivity of EPZ004777 for DOT1L was attributed to its interactions with the hydrophobic pocket. PRMTs and DOT1L belong to the class I methyltransferases of a Rossmann fold[20]. Because the class I Rossmann fold methyltransferases have the conserved SAM binding sites, we speculate that a similar hydrophobic pocket may also exist in other class I

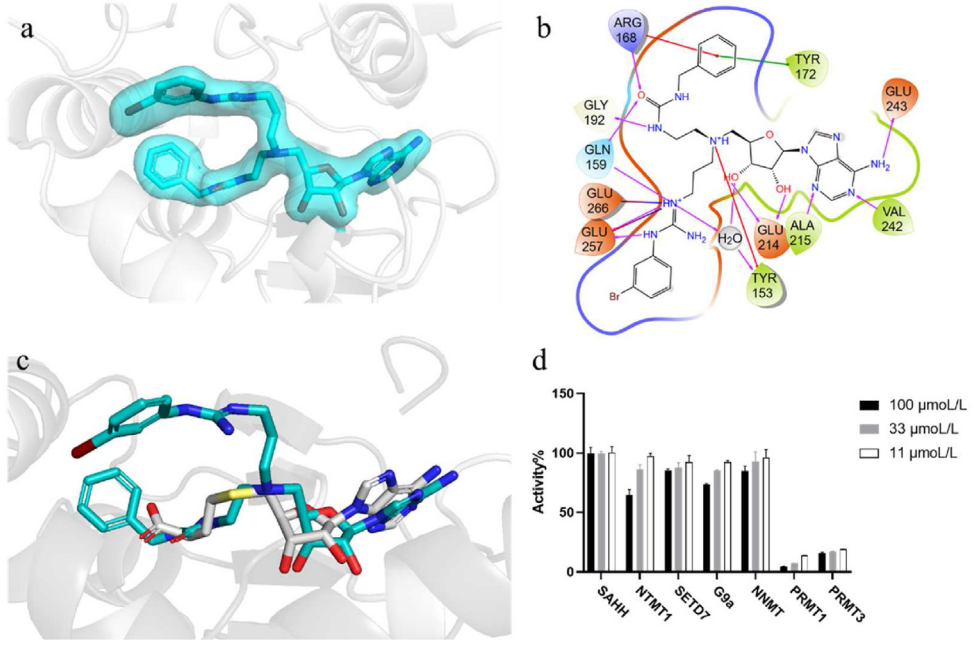

Figure 8 X-ray co-crystal structure of PRMT4 (gray cartoon) complexed with YD1290 (light blue stick, PDB ID: 8G2I). (a, b) Co-crystal structure and molecular interactions of YD1290 with PRMT4. A 2*F*o−*F*c omit map contoured to 1.0 σ is shown for YD1290 as a transparent light blue isosurface. (c) Structure alignment of YD1290 and SAH. (d) Selectivity study of YD1290 on seven in-house methyltransferases and SAHH. All experiments were performed in duplicate ($n = 3$).

methyltransferases[21,22]. Meanwhile, the structural similarities between YD1113 and EPZ004777 suggest that benzyl or phenyl urea are potential pharmacophores to explore the hydrophobic pocket, and may also be adapted and tuned to discover potent inhibitors for PRMTs.

4. Experimental

4.1. Synthesis and characterization of the target compounds

Experimental details of the synthetic works were included in the Supporting Information.

4.2. Protein expression and purification

PRMT1, PRMT3, PRMT4, SAHH, NTMT1, G9a, SETD7 and NNMT were expressed and purified as reported before[9,12]. Proteins (PRMT 1 to PRMT8) used for selectivity assay were expressed and purified by Reaction Biology Corp[23–27].

PRMT3 (residues 211−531) was cloned into the pET28a-MHL expression vector for protein production. The recombinant plasmid was transformed into *Escherichia coli* BL21(DE3). Proteins were overexpressed in Terrific Broth medium and induced with 0.15 mmol/L IPTG at 16 °C overnight. PRMT4 (residues 140−480) was cloned into the pFBOH-MHL vector and expressed in *Sf9* insect cells. After sonification, proteins were purified by Ni-NTA agarose column and eluted with the elution buffer (20 mmol/L Tris-HCl pH 8.0, 100 mmol/L NaCl, 400 mmol/L imidazole). Subsequently, the eluted sample flowed through a HiTrapTM Q HP column (GE Healthcare) pre-equilibrated with 20 mmol/L Tris-HCl pH 8.0, 100 mmol/L NaCl. The sample was then purified by Superdex 200 10/300 (GE Healthcare). The gel-filtration buffer was 20 mmol/L Tris-HCl pH 8.0, 100 mmol/L NaCl, 1 mmol/L DTT. PRMT3 peak fractions were collected and concentrated to 10 mg/mL for crystallization. PRMT4 was prepared the same as PRMT3, though PRMT4 was concentrated to 18 mg/mL for crystallization.

4.3. Inhibition activity of the target compounds

A fluorescence-based SAHH-coupled assay was applied to study the inhibition activity of all synthesized compounds on PRMT1 and 3. For selectivity studies, inhibition was performed through a radioactive assay at Reaction Biology Corp.

The PRMT1 methylation assay was performed under the following conditions in a final well volume of 100 μL: 2.5 mmol/L HEPES (pH = 7.0), 25 mmol/L NaCl, 25 μmol/L EDTA, 50 μmol/L TCEP, 0.01% Triton X-100, 5 μmol/L SAHH, 0.1 μmol/L PRMT1, 10 μmol/L AdoMet, and 10 μmol/L ThioGlo4. After incubating with the inhibitors for 10 min at 37 °C, reactions were initiated by the addition of 5 μmol/L H4-21 peptide (K_m value). The fluorescence signal was monitored on a BMG CLARIOstar microplate reader with excitation at 400 nm and emission at 460 nm for 15 min. Data were processed using GraphPad Prism software 8.0. The IC_{50} values were calculated with Eq. (1):

$$Y = \text{Bottom} + (\text{Top} - \text{Bottom})/(1 + (IC_{50}/X)^{\wedge}\text{HillSlope}) \quad (1)$$

where X is the inhibitor concentration, Y is the response, Top and Bottom is the plateaus of the curve, HillSlope is the slope factor.

The PRMT3 methylation assay was performed under the following conditions in a final well volume of 100 μL: 20 mmol/L Tris (pH = 7.5), 0.01% Triton X-100, 5 μmol/L SAHH, 0.25 μmol/L PRMT3, 30 μmol/L AdoMet, and 15 μmol/L ThioGlo4. After incubating with the inhibitors for 10 min at 30 °C, reactions were initiated by the addition of 30 μmol/L H4-21 peptide (K_m value). Fluorescence was monitored on a BMG CLARIOstar microplate reader with excitation 400 nm and emission 460 nm. Data were processed by using GraphPad Prism software 8.0. The IC_{50} values were calculated with the same method as PRMT1. All experiments were performed in triplicate.

4.4. Inhibition mechanism study

The inhibition mechanism of YD1113 on PRMT3 was studied with the fluorescence-based SAHH-coupled assay. Varying concentrations of SAM (from 30 to 240 μmol/L) with 30 μmol/L fixed concentration of H4-21 or varying concentration of H4-21 (from 15 to 240 μmol/L) with 30 μmol/L fixed concentration of SAM were included in reactions at concentration of YD1113 ranging from 1.5 nmol/L to 100 μmol/L.

The inhibition mechanism of YD1290 was study on PRMT1 with the fluorescence-based SAHH-coupled assay. Varying concentrations of SAM (from 5 to 40 μmol/L) with 4 μmol/L fixed concentration of H4-21 or varying concentration of H4-21 (from 4 to 32 μmol/L) with 5 μmol/L fixed concentration of SAM were included in reactions at concentration of YD1290 ranging from 0.15 nmol/L to 10 μmol/L.

All the IC_{50} values were determined in triplicate. Fluorescence was monitored on a BMG CLARIOstar microplate reader with excitation 400 nm and emission 460 nm. Data were processed by using GraphPad Prism software 8.0. The IC_{50} values were calculated with the same method as the inhibition study on PRMT1.

4.5. Selectivity study

A fluorescence-based SAHH-coupled assay was applied to study the effect of the compound on methyltransferase activity of NTMT1, SETD7, G9a, NNMT, tbPRMT7 and SAHH. For NTMT1, the assay was performed in a final well volume of 100 μL: 25 mmol/L Tris (pH = 7.5), 50 mmol/L KCl, 0.01% Triton X-100, 5 μmol/L SAHH, 0.1 μmol/L NTMT1, 3 μmol/L AdoMet, and 10 μmol/L ThioGlo4. After incubation for 10 min with the inhibitor, reactions were initiated by the addition of 0.5 μmol/L GPKRIA peptide, and the reaction was monitored for 15 min. For SETD7, the assay was performed in a final well volume of 100 μL: 25 mmol/L potassium phosphate buffer (pH = 7.6), 0.01% Triton X-100, 5 μmol/L SAHH, 1 μmol/L SETD7, 2 μmol/L AdoMet, and 10 μmol/L ThioGlo4. After incubation for 10 min with the inhibitor, reactions were initiated by the addition of 90 μmol/L H3-21 peptide, and the reaction was monitored for 15 min. For G9a, the assay was performed in a final well volume of 100 μL: 25 mmol/L potassium phosphate buffer (pH = 7.6), 1 mmol/L EDTA, 2 mmol/L MgCl2, 0.01% Triton X-100, 5 μmol/L SAHH, 0.1 μmol/L His-G9a, 10 μmol/L AdoMet, and 10 μmol/L ThioGlo4. For NNMT, the assay was performed in a final well volume of 100 μL: 25 mmol/L Tris (pH = 7.5), 50 mmol/L KCl, 0.01% Triton X-100, 5 μmol/L SAHH, 0.1 μmol/L NNMT, 10 μmol/L AdoMet, and 10 μmol/L ThioGlo4. After incubation for 10 min with the inhibitor, reactions were initiated by the addition of 10 μmol/L nicotinamide, and the reaction was

monitored for 18 min. For *Tb*PRMT7, the assay was performed in a final well volume of 100 μL: 25 mmol/L Tris (pH = 7.5), 50 mmol/L KCl, 0.01% Triton X-100, 5 μmol/L SAHH, 0.2 μmol/L PRMT7, 3 μmol/L AdoMet, and 15 μmol/L ThioGlo4. After incubation for 10 min with the inhibitor, reactions were initiated by the addition of 60 μmol/L H4-21 peptide, and the reaction was monitored for 15 min. For The inhibitors were added at three concentrations: 100, 33.3, 11.1 μmol/L.

The effect of the inhibitors on the coupled enzyme, SAHH, was also evaluated. The assay was performed in a final well volume of 100 μL: 25 mmol/L Tris (pH = 7.5), 50 mmol/L KCl, 0.01% Triton X-100, 0.1 μmol/L SAHH, and 15 μmol/L ThioGlo4. After incubation for 10 min with the compound, 0.5 μmol/L SAH was added to initiate the reactions.

All experiments were performed in duplicate. Fluorescence was monitored on a BMG CLARIOstar microplate reader with excitation at 400 nm and emission at 460 nm.

The selectivity of compounds YD1113 and YD1290 on PRMTs were performed by Reaction Biology Corp. For PRMT1, 5 nmol/L protein, 1.5 μmol/L Histone H4 and 1 μmol/L SAM were used. For PRMT3 to PRMT8, the protein concentration is 60, 5, 1, 10, 60 and 80 nmol/L. And 1.5 of μmol/L Histone H4 and 1 μmol/L of SAM were used for PRMT3 to PRMT8. The IC_{50} values of YD1290 on PRMT1, 3, 4, 6 and 8 were calculated with least squares fit.

4.6. Thermal shift assay

The fluorescence-based thermal shift assay was performed using a StepOne plus qPCR instrument (Thermal Fisher). For PRMT1, 10 μmol/L of protein was mixed with 2x sypro orange and DMSO, or 100 μmol/L SAM, or 100 μmol/L YD1113, or 100 μmol/L YD1290 in a buffer consisting of 2.5 mmol/L HEPES (pH = 7.0), 25 mmol/L NaCl, 25 μmol/L EDTA, 50 μmol/L TCEP, 0.01% Triton X-100. For PRMT3, 20 μmol/L of protein was mixed with 2x sypro orange and DMSO, or 100 μmol/L SAM, or 100 μmol/L YD1113, or 100 μmol/L YD1290 in a buffer consisting of 20 mmol/L Tris (pH = 7.5), 0.01% Triton X-100. For PRMT4, 20 μmol/L of protein was mixed with 2x sypro orange and DMSO, or 100 μmol/L SAM, or 100 μmol/L YD1113, or 100 μmol/L YD1290 in a buffer consisting of 20 mmol/L bicine (pH = 8.5), 0.01% Triton X-100. All samples were heated from 25 to 75 °C at an increased rate of 0.5 °C per minute. Protein denaturation was monitored by the increased fluorescence signal of Sypro Orange, which captures exposed hydrophobic residues during thermal unfolding. The recorded curves were analyzed by the software StepOne plus and plotted in GraphPad Prism 8 software.

4.7. Co-crystallization and structure determination

Proteins were incubated with compounds at a 1:2 M ratio for 0.5 h on ice. Afterwards, protein-compound complexes were crystallized by sitting drop vapor diffusion method with mixing 1 μL proteins and 1 μL reservoir solutions. The crystals of PRMT3-II710 were grown in 20% PEG3350, 0.3 mol/L sodium formate. The crystals of PRMT3-YD1113 were obtained in 0.1 mol/L Tris-HCl (pH 8.5), 2.0 mol/L ammonium sulfate. The PRMT4-YD1113 was crystallized in 0.2 mol/L calcium chloride dihydrate, 0.05 mol/L HEPES sodium pH 7.5, 28% *v*/*v* polyethylene glycol 400, 0.002 mol/L spermine. The PRMT4-YD1290 was crystallized in 0.1 mol/L BICINE pH 9.0, 2.0 mol/L magnesium chloride hexahydrate. The crystals were flash-frozen in liquid nitrogen using a cryoprotectant consisting for reservoir solution supplemented with 15% glycerol.

X-ray diffraction data for both PRMT3+YD1113, II710 and PRMT4+YD1290, YD1113 were collected at 100 K on the 24ID-E or 24ID-C of NCAT at Advanced Photon Source (APS), Argonne National Laboratory and all the data was processed using the HKL-3000 suite[28].

All 4 structures were solved by molecular replacement using PHASER with PDB entry 2FYT and 5U4X as search template for PRMT3 and PRMT4 respectively. REFMAC was used for all structure refinement[29,30]. Geometry restraints for all compound refinement were prepared with by GRADE developed at Global Phasing Ltd.[31]. Graphics program COOT was used for all model building and visualization[32]. MOLPROBITY was used for structure validation[33].

4.8. Structural alignment of PRMT3 with other PRMTs

Structural alignment of PRMT3 with other PRMTs were taken with the protein structure alignment module in Maestro 12.8. The structures and interaction diagram were drawn with Maestro. PRMT1 (PDB ID, 6NT2), PRMT4 (PDB ID, 5IH3), PRMT5 (PDB ID, 4X63), PRMT6 (PDB ID, 4Y2H), PRMT7 (PDB ID, 4C4A) and PRMT8 (PDB ID, 4X41) were obtained from protein data bank (www.rcsb.org).

4.9. Cell permeability evaluation by MALDI-MS

The triple negative breast cancer cell line MDA-MB-231 was cultured in RPMI media supplemented with 10% fetal bovine serum and 1% Penn-Strep (Gibco). The cells were cultured in tissue culture dish (Falcon 353003). Cells were maintained in cell culture flasks until seeding into a 24 well tissue culture plate (Falcon 353047) at a density of 0.1×10^6 cells/mL and incubated overnight at 37 °C, 5% CO_2, and 95% humidity, with the lid on. The cells were then treated with YD1290 at 100 and 10 μmol/L concentrations, and incubation was continued for the specified time. The cell permeable control peptide was also incubated at 1 μmol/L concentration. After incubation, the media was removed, and the cells were washed with 1 × PBS three times to remove any residual compound or peptide attached to the cell surface. Then, 100 μL of 1 × PBS was added, and the cells were snap frozen in liquid nitrogen twice. The cell lysate was then analyzed with MALDI using DHB matrix to identify the presence of the compound inside the cell.

4.10. Accession codes

The coordinates for the complexed structures of human PRMT3-II710 (PDB ID: 8G2F), PRMT3-YD1113 (PDB ID: 8G2G), PRMT4-YD1113 (PDB ID: 8G2H), and PRMT4-YD1290 (PDB ID: 8G2I) have been deposited in the Protein Data Bank. Authors will release the atomic coordinates and experimental data upon article publication.

Acknowledgments

We are grateful to Purdue University Faculty Scholar program from the Ralph W. and Grace M. Showalter Trust and Department of Medicinal Chemistry and Molecular Pharmacology (to Rong Huang). The SGC is a registered charity (number 1097737)

that receives funds from AbbVie, Bayer Pharma AG, Boehringer Ingelheim, Canada Foundation for Innovation, ikEsheiklman Institute for Innovation, Genome Canada through Ontario Genomics Institute [OGI-055], Innovative Medicines Initiative (EU/EFPIA) [ULTRA-DD grant no. 115766], Janssen, Merck KGaA, Darmstadt, Germany, MSD, Novartis Pharma AG, Ontario Ministry of Research, Innovation and Science (MRIS), Pfizer, São Paulo Research Foundation-FAPESP, Takeda, and Wellcome. We also appreciate valuable feedback from Dr. Akshay S. Kulkarni. This work was supported by Purdue University Faculty Scholar program from the Ralph W. and Grace M. Showalter Trust and Department of Medicinal Chemistry and Molecular Pharmacology (to Rong Huang). The authors acknowledge the support from NIH P30 CA023168 (Purdue University Center for Cancer Research), and the NSERC grant (RGPIN-2021-02728 (Jinrong Min)).

Author contributions

Youchao Deng designed and synthesized compounds, purified PRMT3, performed the inhibition characterization, and wrote the manuscript; Xiaosheng Song performed PRMT3 and 4 purification, crystallization, and X-ray data collection; Iredia D. Iyamua synthesized and characterized II710, and performed cell permeability experiments; Aiping Dong collected the diffraction data and determined the crystal structures; Jinrong Min provided supervision of crystallization and funding acquisition; Rong Huang conceived and directed the project conceptualization and project administration, reviewed and edited the manuscript, and provided funding acquisition. All authors provided critical feedback and have approved the final version of the manuscript.

Conflict of interest

The authors declare no competing financial interest.

Appendix A. Supporting information

Supporting data to this article can be found online at https://doi.org/10.1016/j.apsb.2023.07.022.

References

1. Zurita-Lopez CI, Sandberg T, Kelly R, Clarke SG. Human protein arginine methyltransferase 7 (PRMT7) is a type III enzyme forming ω-NG-monomethylated arginine residues. *J Biol Chem* 2012;**287**:7859−70.
2. Yang Y, Bedford MT. Protein arginine methyltransferases and cancer. *Nat Rev Cancer* 2013;**13**:37−50.
3. Krause CD, Yang ZH, Kim YS, Lee JH, Cook JR, Pestka S. Protein arginine methyltransferases: evolution and assessment of their pharmacological and therapeutic potential. *Pharmacol Ther* 2007;**113**:50−87.
4. Bedford MT, Clarke SG. Protein arginine methylation in mammals: who, what, and why. *Mol Cell* 2009;**33**:1−13.
5. Blanc RS, Richard S. Arginine methylation: the coming of age. *Mol Cell* 2017;**65**:8−24.
6. Al-Hamashi AA, Diaz K, Huang R. Non-histone arginine methylation by protein arginine methyltransferases. *Curr Protein Pept Sci* 2020;**21**:699−712.
7. Brehmer D, Beke L, Wu T, Millar HJ, Moy C, Sun W, et al. Discovery and pharmacological characterization of JNJ-64619178, a novel small-molecule inhibitor of PRMT5 with potent antitumor activity. *Mol Cancer Ther* 2021;**20**:2317−28.
8. Szewczyk MM, Ishikawa Y, Organ S, Sakai N, Li F, Halabelian L, et al. Pharmacological inhibition of PRMT7 links arginine monomethylation to the cellular stress response. *Nate comm* 2020;**11**:1−15.
9. Iyamu ID, Al-Hamashi AA, Huang R. A Pan-inhibitor for protein arginine methyltransferase family enzymes. *Biomolecules* 2021;**11**:854.
10. Cai XC, Zhang T, Kim EJ, Jiang M, Wang K, Wang J, et al. A chemical probe of CARM1 alters epigenetic plasticity against breast cancer cell invasion. *Elife* 2019;**8**:e47110.
11. Gunnell EA, Al-Noori A, Muhsen U, Davies CC, Dowden J, Dreveny I. Structural and biochemical evaluation of bisubstrate inhibitors of protein arginine *N*-methyltransferases PRMT1 and CARM1 (PRMT4). *Biochem J* 2020;**477**:787−800.
12. Al-Hamashi AA, Chen D, Deng Y, Dong G, Huang R. Discovery of a potent and dual-selective bisubstrate inhibitor for protein arginine methyltransferase 4/5. *Acta Pharm Sin B* 2021;**11**:2709−18.
13. Smil D, Eram MS, Li F, Kennedy S, Szewczyk MM, Brown PJ, et al. Discovery of a dual PRMT5-PRMT7 inhibitor. *ACS Med Chem Lett* 2015;**6**:408−12.
14. Chen D, Dong C, Dong G, Srinivasan K, Min J, Noinaj N, et al. Probing the plasticity in the active site of protein N-terminal methyltransferase 1 using bisubstrate analogues. *J Med Chem* 2020;**63**:8419−31.
15. Zhang G, Huang R. Facile synthesis of SAM−peptide conjugates through alkyl linkers targeting protein N-terminal methyltransferase 1. *RSC Adv* 2016;**6**:6768−71.
16. Tewary SK, Zheng YG, Ho MC. Protein arginine methyltransferases: insights into the enzyme structure and mechanism at the atomic level. *Cell Mol Life Sci* 2019;**76**:2917−32.
17. Richardson SL, Mao Y, Zhang G, Hanjra P, Peterson DL, Huang R. Kinetic mechanism of protein N-terminal methyltransferase 1. *J Biol Chem* 2015;**290**:11601−10.
18. Basavapathruni A, Jin L, Daigle SR, Majer CR, Therkelsen CA, Wigle TJ, et al. Conformational adaptation drives potent, selective and durable inhibition of the human protein methyltransferase DOT1L. *Chem Biol Drug Des* 2012;**80**:971−80.
19. Yu W, Chory EJ, Wernimont AK, Tempel W, Scopton A, Federation A, et al. Catalytic site remodelling of the DOT1L methyltransferase by selective inhibitors. *Nat Commun* 2012;**3**:1288.
20. Campagna-Slater V, Mok MW, Nguyen KT, Feher M, Najmanovich R, Schapira M. Structural chemistry of the histone methyltransferases cofactor binding site. *J Chem Inf Model* 2011;**51**:612−23.
21. Konc J, Janezic D. ProBiS algorithm for detection of structurally similar protein binding sites by local structural alignment. *Bioinformatics* 2010;**26**:1160−8.
22. Konc J, ProBiS Janezic D. A web server for detection of structurally similar protein binding sites. *Nucleic Acids Res* 2010;**38**:W436−40.
23. Lee J, Sayegh J, Daniel J, Clarke S, Bedford MT. PRMT8, a new membrane-bound tissue-specific member of the protein arginine methyltransferase family. *J Biol Chem* 2005;**280**:32890−6.
24. Miranda TB, Miranda M, Frankel A, Clarke S. PRMT7 is a member of the protein arginine methyltransferase family with a distinct substrate specificity. *J Biol Chem* 2004;**279**:22902−7.
25. Frankel A, Yadav N, Lee J, Branscombe TL, Clarke S, Bedford MT. The novel human protein arginine *N*-methyltransferase PRMT6 is a nuclear enzyme displaying unique substrate specificity. *J Biol Chem* 2002;**277**:3537−43.
26. Branscombe TL, Frankel A, Lee JH, Cook JR, Yang ZH, Pestka S, et al. PRMT5 (Janus kinase-binding protein 1) catalyzes the formation of symmetric dimethylarginine residues in proteins. *J Biol Chem* 2001;**276**:32971−6.
27. Chen D, Ma H, Hong H, Koh SS, Huang SM, Schurter BT, et al. Regulation of transcription by a protein methyltransferase. *Science* 1999;**284**:2174−7.
28. Otwinowski Z, Minor W. Processing of X-ray diffraction data collected in oscillation mode. *Methods Enzymol* 1997;**276**:307−26.

29. McCoy AJ, Grosse-Kunstleve RW, Adams PD, Winn MD, Storoni LC, Read RJ. Phaser crystallographic software. *J Appl Crystallogr* 2007; **40**:658−74.
30. Murshudov GN, Vagin AA, Dodson EJ. Refinement of macromolecular structures by the maximum-likelihood method. *Acta Crystallogr D Biol Crystallogr* 1997;**53**:240−55.
31. Smart OS, Womack TO, Flensburg C, Keller P, Paciorek W, Sharff A, et al. Exploiting structure similarity in refinement: automated NCS and target-structure restraints in BUSTER. *Acta Crystallogr D Biol Crystallogr* 2012;**68**:368−80.
32. Emsley P, Cowtan K. Coot: model-building tools for molecular graphics. *Acta Crystallogr D Biol Crystallogr* 2004;**60**:2126−32.
33. Davis IW, Murray LW, Richardson JS, Richardson DC. MOLPROBITY: structure validation and all-atom contact analysis for nucleic acids and their complexes. *Nucleic Acids Res* 2004;**32**: W615−9.